

2. ACCELERATOR AUGMENTATION PROGRAM

2.1 LINAC

S. Ghosh, A. Rai, P. Patra, G.K. Chowdhury, B.K. Sahu, A. Pandey, D.S. Mathuria, J.Karmakar, S.S.K.Sonti, K.K.Mistry, R.N.Dutt, J.Chacko, A.Chowdhury, S.Kar, S.Babu, M.Kumar, J.Antony, J.Zacharias, P.N.Prakash, T.S.Datta, D.Kanjilal and A.Roy

2.1.1 Delivery of ion beams from Pelletron and LINAC for Nuclear Physics experiment

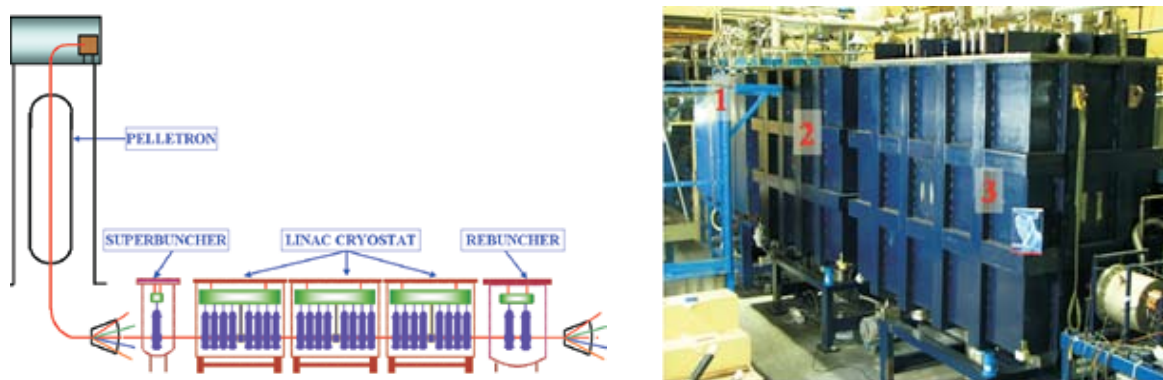


Fig. 1. The schematic of the Pelletron and Superconducting Linear accelerator of IUAC. The second picture shows the three LINAC cryostats installed in the beam line

The Pelletron accelerator and the first accelerating module of LINAC along with its superbuncher and Rebuncher are being used to deliver ion beams for experiments in beam Hall-2. The first component of the superconducting LINAC is the superbuncher cryostat having a single niobium Quarter Wave Resonator (QWR) followed by three accelerating modules, each containing eight QWRs and a rebuncher cryostat housing two QWRs. The complete layout of the Pelletron and LINAC is given in figure 1. The remaining two accelerating modules of LINAC are installed and aligned in the beam line (figure 1). The fabrication work of the indigenous resonators to be installed in LINAC cryostat 2 and 3 is almost complete and cold tests of the cavities are going on in test cryostat. Soon the indigenous resonators will be installed in the last two cryostats and beam will be accelerated through the complete LINAC. Meanwhile, different beams have been accelerated by the first module of LINAC and delivered to perform experiments with HYRA, NAND and other detection systems.

During the last LINAC acceleration during the period of July-September 2010, all eight resonators of the first accelerating module of LINAC were used in beam

acceleration. The accelerating fields at 6 watts of input power during Q-measurement and the phase locked fields of the resonators at the time of beam acceleration are shown in figure 2. It is to be noted here that the forward RF power used to phase lock the resonators was around 100 watts and about 150 watts would be required if a resonator was to be phase locked at a similar field what was obtained at 6 watts of input power. In order to operate the LINAC for longer duration extending for a few months without degrading the performance, it was decided that the resonator would be phase locked without exceeding the forward RF power beyond 100 watts. Consequently, at the time of beam acceleration, the resonators were phase locked at the accelerating fields lower than the values obtained at 6W of input power during Q-measurement. In future, to phase lock the resonators at higher fields, forward RF power exceeding 100 watts will be required and for this, use of a semi rigid cable to carry the RF power and possibility of electronic damping of the microphonics present in a resonator are being planned. During this period, three ion beams were accelerated and delivered in HYRA and NAND beam line, the details are given in Table – 1.

Beam	Pell. Energy (MeV)	E-gain (LINAC-1) (MeV)	Beam Line
$^{16}\text{O}^{+8}$	100	26	HYRA
$^{16}\text{O}^{+8}$	96	24	NAND
$^{19}\text{F}^{+9}$	115	25	NAND
$^{30}\text{Si}^{+11}$	126	40	HYRA

Table 1. Beam species accelerated through the first accelerating module of LINAC

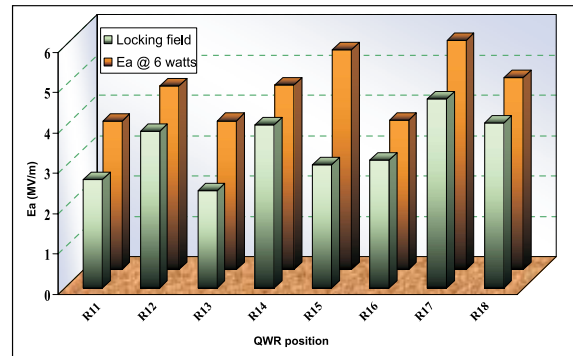


Fig. 2. The accelerating fields at 6 W and at the time of beam acceleration

2.1.2 Role of random phase focusing on the time width of the beam bunch at LINAC exit

At the time of beam acceleration through LINAC, usually the phase of the synchronous particle at the middle of the first accelerating gap of a QWR is always kept at $\sin(70)$ (or $\cos(-20)$) to ensure phase focussing in the longitudinal phase space along with the acceleration. But if the beam is to be transported a long distance after LINAC, then changing the synchronous phase of a few resonators from 70° to 110° is found to be more beneficial to accomplish the time focussing of the beam bunch. To understand this phenomenon, a simulation code was written to calculate the combination of synchronous phases to be applied on the resonators to obtain the minimum time width of the beam bunch at the target location which is ~ 30 metres from the exit of the first LINAC module [9]. The calculation showed that for 96 MeV $^{16}\text{O}^{+8}$ beam from Pelletron, the minimum time width of the beam bunch would be obtained when the fourth resonator of LINAC-1

would be kept at 110° with the remaining resonators kept at 70° . During the LINAC acceleration, the time width of the same beam with same energy was measured at the final scattering chamber when all the resonators are kept at 70° in one case and with only the fourth resonator kept at 110° in the other case. In the latter case, a reduction of $\sim 20\%$ in the time width of the beam bunch was measured at the target.

2.1.3 Use of last accelerating resonators as the re-buncher

During the last LINAC operation concluded in 2010, the rebuncher could not be operated due to shortage of liquid helium. So the same simulation code was used to find out whether the last LINAC resonator could be used as a rebuncher to control the time width of the beam bunch at the target. For $^{16}\text{O}^{+8}$ and $^{19}\text{F}^{+9}$ beams with fixed energy from Pelletron and variable energy gain from LINAC, a reduction of time width in the range of 33% to 62% was measured after applying the calculated bunching field on the last LINAC resonator acting as a rebuncher. Without this provision, the time width of the beam bunch increased to ~ 2.2 ns, which was too large to conduct the experiments. However, with the help of the last resonator as rebuncher, the time width was restricted to a value of 0.5 to 1.5 ns on all the occasions.

2.1.4 Status of automation of LINAC operation

To ensure a safe operation of LINAC with minimum human intervention, a number of steps were taken to automate the LINAC operation. The different developments in the automation of LINAC operation are as follows:

- (a) Remote control of the phase/amplitude locking of a superconducting resonator was implemented. This had helped to control LINAC and Pelletron simultaneously with reduced effort at the time of beam delivery.
- (b) During the phase locking of the resonator, the amount of forward power going to a resonator is monitored in a module and displayed in the control console kept at the control room and other places.
- (c) In the event of the resonator going out of phase lock, RF power going to the resonator from the amplifier reaches its maximum value which may damage the power cables. A code in python is written to monitor the status of the phase lock condition and to sense the amount of power going in to the resonators. Whenever a resonator goes out of lock and RF power from amplifier goes high for more than a minute, the phase and amplitude locks of the resonator are switched off by the code to reduce the RF power and to protect the power cable.
- (d) The movement of the drive coupler to feed the power in to a resonator is now controlled by computer with a position read back of the power coupler.

- (e) An electronic device containing multiple outputs of pulse signal necessary for conducting simultaneous RF pulse conditioning of the resonators was fabricated and used during last LINAC operation. Each channel of the module is computer controlled with an option to vary their duty cycle etc.

The automation process for the LINAC operation will be further improved and a Piezo-actuator based tuning mechanism will replace the existing helium gas based arrangements.

2.1.5 Superconducting Niobium Resonators

P.N. Prakash, K.K. Mistri, S.S.K. Sonti, A.Rai, J.Zacharias, S.Ghosh, P.Patra, G.K.Chowdhury, D.S.Mathuria, R.N.Dutt, A.Pandey, B.K.Sahu, D.Kanjilal & A.Roy

Several QWRs from the production batch were tested at 4.5 K and the results achieved have been excellent. The low beta resonator design has been completed and a room temperature copper model was built to validate the electromagnetic parameters. Two prototype niobium low beta resonators are presently under construction. Fabrication of the Single Spoke Resonators for Project-X at Fermi National Accelerator Laboratory (FNAL) is in advanced stage. Both the TESLA-type single cell cavities, which were fabricated last year, were tested at 2 K and they have shown good performance. Based on the lessons learned from the initial fabrication, two improved single cell cavities are being built. In addition there are plans to build a 5-cell cavity and a 650 MHz $\beta=0.9$ single cell cavity.

2.1.5.1 Performance of Production Resonators

Several QWRs from the resonator production were tested at 4.5 K to check their performance. In figure 1, results from the off-line testing of the resonators, is shown. The

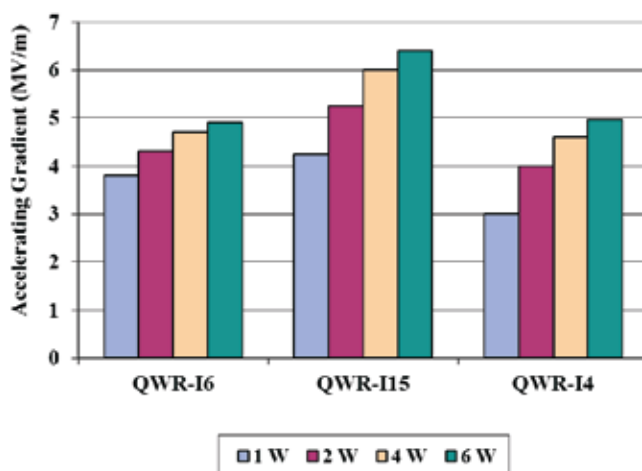


Fig. 1. Comparative performance of three resonators at different input power levels

nominal design goal is to reach an accelerating gradient of 4 MV/m at 4 W of rf power, which is easily achieved.

2.1.5.2 Low Beta Resonator

The proposed High Current Injector system at IUAC will consist of several accelerating structures including a superconducting low beta module, containing niobium resonators. For this, a low beta resonator has been designed which is optimized for



Parameter	Value
f	97 MHz
β_0	0.05
L_{eff}	10.4 cm
U_0	26 mJ
B_{peak}	64 G
E_{peak}	3.4 MV/m
R_{sh}/Q	650 Ω
QR_s	16.1

Fig. 2. Low beta resonator (left) and design parameters (right)



	Calculated	Measured
f	92.54 MHz	92.25 MHz
β_0	0.051	0.051
U_0	28.7 mJ	27 mJ
R_{sh}/Q	650 Ω	658 Ω
Δf_{ST}	100 kHz	110 kHz

Fig. 3. Copper model of the low beta resonator showing the central conductor and resonator (left). Parameters of the copper model (right). The calculated values shown are calculated for the drift tube design used on the copper model, and not the actual design

$\beta=0.05$, operating at 97 MHz. The resonator has been modelled using CST-Microwave Studio and optimized to reduce the peak electric and magnetic fields while maintaining high values for the shunt impedance and geometry factor. The mechanical analysis has been done using ANSYS multiphysics code. In figure 2 the low beta resonator and its electromagnetic parameters are shown.

In order to validate the electromagnetic parameters of the low beta resonator design, before constructing the prototype niobium resonators, a copper model was built. In figure 3 the copper resonator and the measured parameters on it, are shown. The measured frequency was lower than the design frequency since the drift tube did not have rounded edges, which resulted in slightly higher drift tube capacitance thereby reducing the frequency.

In figure 4, data from the bead pull measurements on the copper model are shown along with the results from Microwave Studio calculations.

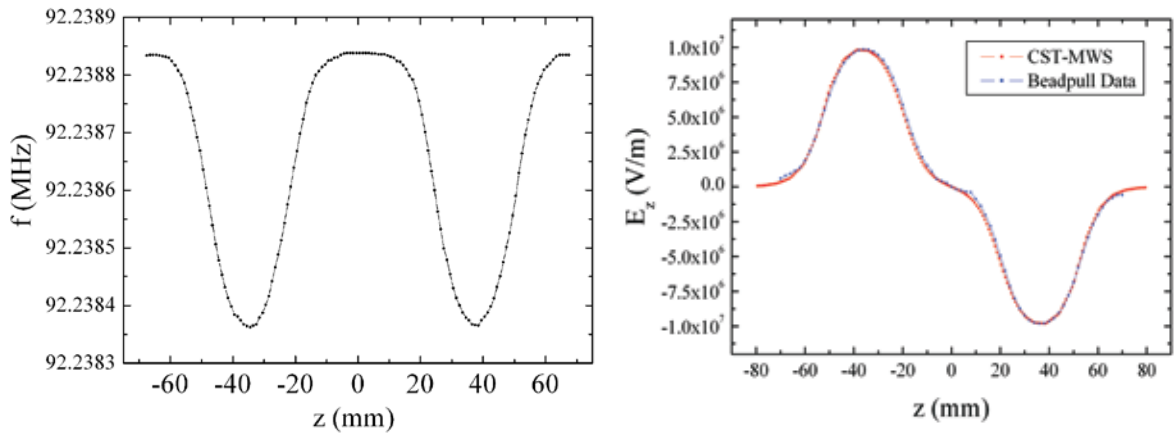


Fig. 4. Bead pull measurement - frequency as a function of length along the beam axis (left). Electric field profile along the beam axis calculated from the bead pull data (right). For comparison the field profile from Microwave Studio simulation is also shown

Presently two niobium prototypes are under fabrication. The outer niobium housings have been rolled and machined. The die for forming the central conductor tapered tube-halves, has been developed. In addition, the dies required for forming the drift tube cup and the saddle shaped housing beam port cup, have also been developed. The niobium drift tubes have been formed and the first set of niobium central conductor taper tubes has also been formed. In figure 5, some of the niobium components for the prototype resonator are shown. We plan to complete the first prototype resonator in the next few months.



Fig. 5. Niobium components for the prototype low beta resonators – Outer Housings (left), Central Conductor halves (center), and saddle shaped Cup for the Beam Port on the Outer Housing (right)

2.1.5.3 Spoke Resonators

Fabrication of the Single Spoke Resonators ($\beta=0.22$, $f=325$ MHz) for Project-X at Fermi National Accelerator Laboratory (FNAL) has been slightly delayed due to some design changes in the resonator, which required development of additional welding fixtures. Electron beam welding of the two spokes, forming of the end walls, welding of the beam ports to the end walls, development of the coupler port pullout followed by actual pullouts on the niobium shells, have been completed. In addition, the donut ribs have been formed and work towards attaching the stiffening ribs on the end walls has progressed.

Due to the design change, welding of the coupler port flange assembly to the outer shell required completely new fixturing. Also, since this joint is accessible from the inside only, it required a tilting fixture. Due to limitation in the chamber height vis-à-vis the outer shell diameter, development of the appropriate fixturing took time. Presently the coupler ports are being welded to the shell. After this the shell assembly would be electropolished. Similarly the end wall and spoke assemblies would be electropolished separately, before completing the resonator assembly. We propose to complete the spoke resonator fabrication in the next 3 months.



Fig. 6. Welded niobium Spoke (left), End Wall with the Beam Port (center), Outer Shell with Coupler Port flanges (right)

2.1.5.4 Single & Multi Cell Cavities

Under the Indian Institutions and Fermi Lab Collaboration (IIFC), Raja Ramanna Centre for Advanced Technology (RRCAT), Indore and IUAC have developed two TESLA-type niobium single cell cavities. After the fabrication, the cavities were sent to Fermi Lab for inspection, processing and testing, which included inspection of the cavity interior surface-in particular the equator joint using the Kyoto camera, centrifugal barrel polishing, electropolishing, heat treatment, high pressure rinsing, 120 °C baking, and performance testing at 2 K. The first cavity could achieve 19 MV/m accelerating gradient whereas the second cavity achieved 21 MV/m accelerating gradient in the first test and after further processing it could go upto 23 MV/m. In figure 7, the performance of the second cavity is shown. The accelerating gradients achieved in the two cavities are consistent with results achieved on the first cavities built anywhere else.

Encouraged by the results, two more improved single cell cavities incorporating all the lessons learnt from the initial experience, are presently under fabrication. The first improved single cell cavity has been completed and the second cavity is in advanced state of completion.

The immediate future plans under the IIFC collaboration include fabrication of a 5-cell 1.3 GHz cavity with simple end tubes. There are plans to separately develop the end groups for this cavity. In addition, we plan to build a single cell 650 MHz, $\beta=0.9$ cavity during the latter part of the year.

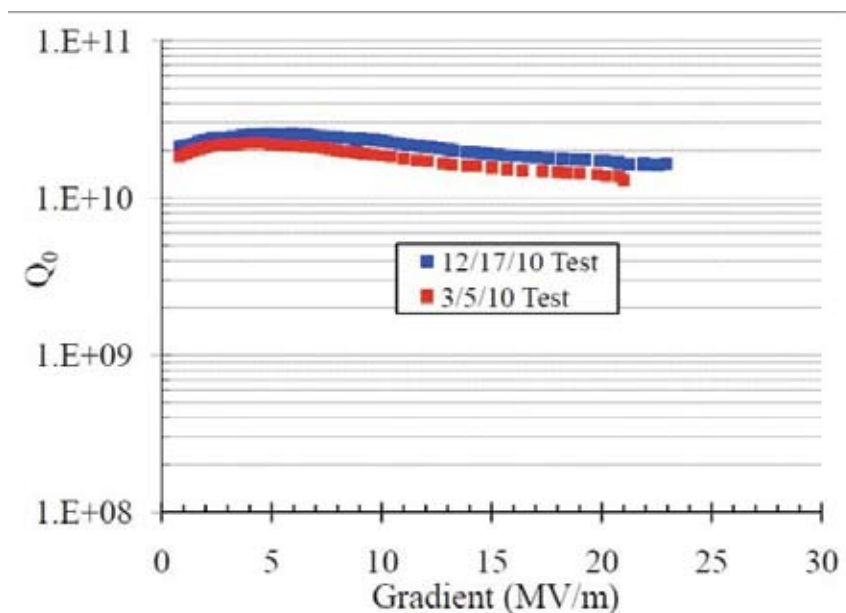


Fig. 7. 2 K test results on the second single cell niobium cavity

2.1.5.5 Facility Upgrade

The SRF infrastructure at IUAC is nearly a decade old. Over this period the facilities have been extensively used for fabricating niobium resonators. At present the control system on the electron beam welding machine runs on a PC and operating system that are obsolete. Several systems in the highly acidic environment of the chemical lab (used for electropolishing) have corroded.

It is essential to maintain the facilities in top condition for fabricating the niobium resonators. The non-availability of key components in these crucial facilities is a serious issue. In view of this we have decided to extensively upgrade the facilities. Keeping in mind the ongoing works and immediate commitments, the upgradation work will be spread over two academic years.

It is planned to replace the control system in the electron beam welding facility using a more modern PC, operating system and control software, along with commercially available CNC systems. At the same time we would like to add additional features in the control program, like recording of real time welding parameters, digital video recording of the entire welding process etc.

In the chemical lab, the fume hood and its drainage system needs to be refurbished. A new class-1000 clean room with separate entrance is planned along with high pressure rinsing system inside it. In addition it is planned to procure a DI water plant and a dedicated ultrasonic cleaner exclusively meant for the post processing of niobium resonators. Some civil and structural changes will also be done, such as double door entry system and new flooring to reduce dust levels inside the chemical lab.

2.2 CRYOGENICS

T.S.Datta, J.Chacko, A .Choudhury, J. Antony, M. Kumar, S. Babu, S.Kar, D.S. Mathuria, R.N.Dutt, P. Konduru, R.G. Sharma and A.Roy

In this academic year, complete cryo-network system which includes liquid helium plant, cryogen distribution network and beam line cryomodules was operated successfully for three months at a stretch to conduct series of experiments with accelerated beam through LINAC. There was a degradation of refrigeration capacity during this long schedule of experiments. After the run, attempt was made to improve the capacity from 120 W to 350 W at 4.2 K by complete overhauling of cold expansion engine. After a successful installation of IInd and IIIrd LINAC modules in the beam line in last year, the partial thermal performance test of both the modules were completed by using newly developed cryoline. To augment the helium refrigeration capacity, purchase order for 750 W capacity plant was placed in favour of M/s Linde, Switzerland. The plant is ready and expected to be commissioned

in October 2011. Technical specification of valve box and cryoline to integrate the new refrigerator with existing cryo distribution network is finalised. For HYRA project, twelve number of superconducting quadrupole coils have been wound and a few of them were successfully tested at 4.2 K. First time in India, the development of warm bore cryogen free superconducting magnet system is completed and tested successfully in this academic year with the financial support from DST.

2.2.1 Cryogenic Facility

I. Liquid Helium Plant

The helium plant was operated ten times in this academic year. These runs consist of three month long LINAC beam run and nine off-line runs for testing the quarter wave resonators and superconducting quadrupole coils. The approximate engine running hour is 2000 hrs and estimated total production of LHe was ~ 180000L. In Fig.1, the yearly LHe production is shown.

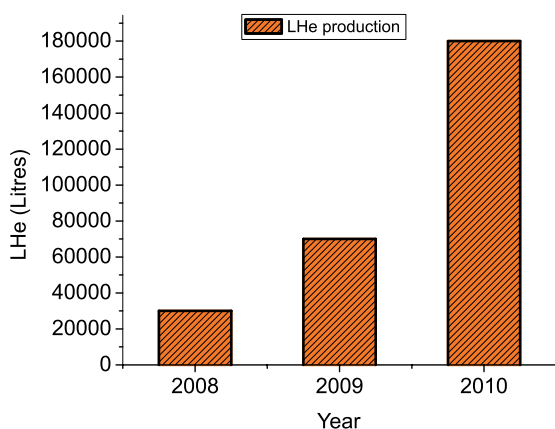


Fig. 1. Yearly LHe Production

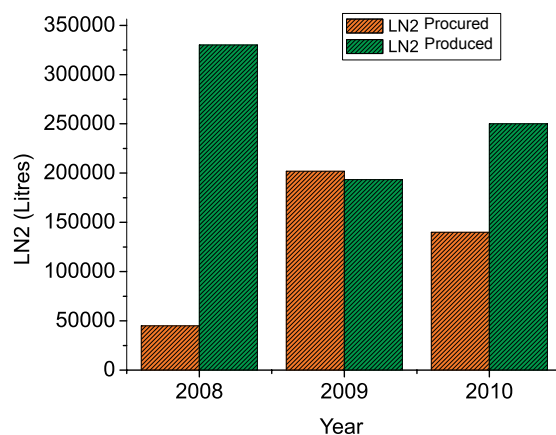


Fig. 2. Yearly LN₂ Production

During the last LINAC run, a gradual degradation of available refrigeration capacity from the plant was noticed. To meet the required demand of dynamic RF load from LINAC cryomodule, the re-buncher cryostat was isolated from cooling network by stopping the LHe supply to the re-buncher cryostat. After the beam test, the performance of the plant was analyzed and the measured available refrigeration capacity was only 120W@ 4.2K. After rectification of cold expansion engine, the refrigeration capacity was improved to 350W.

II. Liquid Nitrogen Plant

In this academic year, total in-house production of LN₂ was 2,50,000 L. Liquid Nitrogen procured from outside vendor was 1,40,000 L. The procurement of LN₂ from

outside vendor was reduced because of enhancement of production capacity from in-house LN2 plant. Fig.2 shows the yearly LN2 production. There was major breakdown maintenance on drier assembly along with regular periodical maintenance of PSA System and cryogenerators in this period.

III. New Liquid Helium Refrigerator

IUAC has planned to procure a new helium refrigerator of guaranteed capacity of 750 watt @ 4.5K to replace the existing helium liquefier for the LINAC system which is more than fourteen years old now. The order for the machine has been placed with M/s LINDE Kryotechnik, Switzerland. The essential features of the refrigerator are (1) fully automated machine varying its capacity from 200-750 W of input power at 4.5 K by using variable frequency drive motor with the compressor, (2) Guaranteed Liquefaction capacity of >180 lph with LN2 precooling, (3) 10 K cool down line having a flow capacity of ~3 g/s for the initial cool down of cryostat and (4) receiving port of cold helium return flow from the cryostats during cool down and normal operations. In Fig.3, the picture of the cold box at vendor's site is shown.



Fig. 3. Picture of the Cold Box of 750 W Helium refrigerator

The order for the plant was placed on March, 2010 and the cold box was recently tested at the factory for its performance. During the factory test, achieved liquefaction rate was ~225 litres per hour and maximum refrigeration capacity was ~1000W which is almost 33% more than the maximum specified capacity. Also the helium compressor has been separately tested at manufacturer's site and the maximum capacity achieved was 110g/s of flow rate at 14bara pressure and the input power was 335 kW (design specification was 106 g/s at 14barg pressure and power input was 315kW). The plant is being currently being packed and shall be shipped in April, 2011.

To make the refrigerator operational here at IUAC site, a number of pre-installation activities have been initiated to complete the commissioning by October 2011. The pre- installation works include room temperature piping jobs connecting the cold box, the compressor and the gas tanks and electrical distribution panel along with UPS and Generator back up. Various options to supply RO quality chilled water for the helium compressor are being discussed and final decision will be taken based on cost, space requirement etc.

2.2.2 LINAC Cryomodule

I. *New helium cooling scheme for LINAC Cryomodule-I*

During last beam test in LINAC, a new helium precooling scheme had been adopted for 1st LINAC cryomodule as earlier option was not available after the installation of additional cryomodules. The new scheme is based on the circulation of evaporated helium gas from liquid helium vessel to the precooling channel. Helium gas flow rate was comparatively less than earlier as the pressure head was limited and subsequently the average cool down rate of resonators was slower than that of earlier cooling rates. This slower cooling rate did not influence the performance of the resonators as there was no obvious deterioration in accelerating field in comparison to the earlier LINAC run. In Fig. 4, the cool down profile of resonators for 1st LINAC cryomodule is shown.

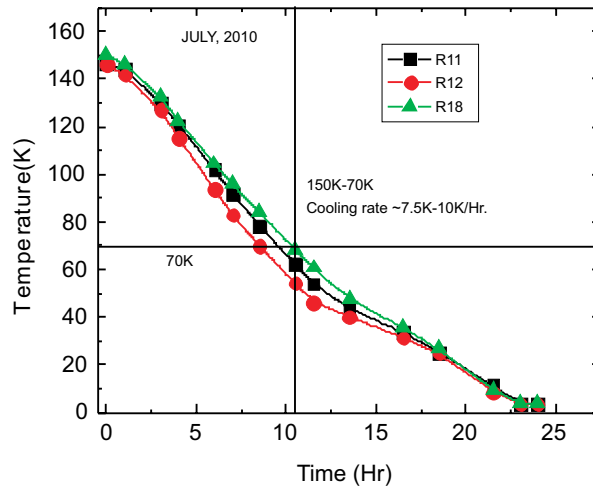


Fig. 4. The cool down profile of LINAC-1

II. *Thermal Performance test of LINAC Cryomodule II & III*

In this academic year, both IInd and IIIrd LINAC cryomodules have been integrated with existing LHe distribution network. In Fig. 5, all the cryomodules integrated with LHe distribution network are shown.



Fig. 5. LINAC II & III cryomodule

The LN2 flow sequence for thermal copper radiation shield of IInd & IIIrd cryomodules is different than that of Ist cryomodule. Extensive studies have been done to generate temperature profile of thermal shield and same is shown in Fig 6a. The LINAC-III module was cooled to 4.2K and measured static heat load without cavities and cavity accessories was 8 – 10 W. The measured data agrees well with the design value. In Fig.6b, the cool down profile of III rd cryomodule is shown.

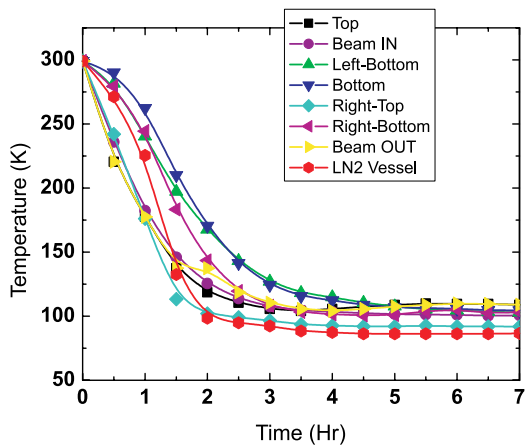


Fig. 6a. Temperature profiles of different surfaces of thermal radiation shield of IInd and IIIrd LINAC module

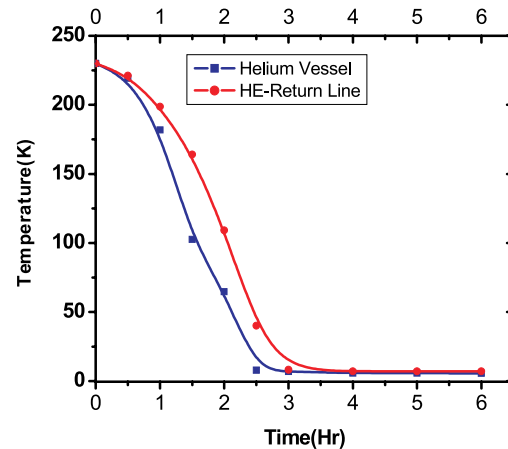


Fig. 6b. Cool Down profile of LHE vessel of IIIrd LINAC Module

2.2.3 Other Development Projects

A. DST Project on Development of 6 Tesla Cryogen free Superconducting Magnet System (CFMS)

First time in India, a warm bore cryogen free superconducting magnet system (CFMS) is developed at IUAC. The CFMS consists of a two stage GM cryocooler, a 6

Tesla superconducting solenoid magnet, Hybrid current leads, and the cryostat. Prior to integrating with cryocooler, the magnet was tested with liquid helium in simple test cryostat. The magnet quenched thrice at three different magnetic fields before reaching 6.2T.

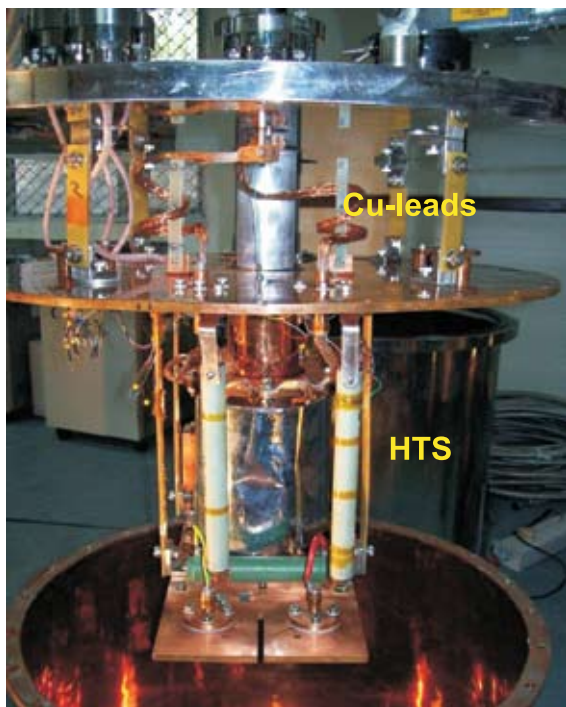


Fig. 7. Internal view of CFMS



Fig. 8. Warm bore Cryogen-free superconducting magnet system

The hybrid current lead consisting of optimized copper leads at the warmer section, high temperature superconducting leads at the intermediate temperature range and finally NbTi at 4.2K have been designed and developed. The superconducting magnet has been integrated with the 2nd stage of the cryocooler by specially designed thermal linkage. The Quench protection system has also been incorporated in the system. The thermal shield and internal components including magnet and the complete system ready for use are shown in Fig. 7 & 8 respectively. The stabilized temperature of magnet and thermal shield is 3.2K and 30K respectively. The typical cool down time is 15Hr. In Fig. 9 the cool down profile of the magnet in CFMS is shown. Thermal stability and quench phenomenon has been studied with different sweep rate. The maximum allowable sweep rate for continuous charging has been determined from the stability study of the magnet. The system is ready for user's experiment. Students from IIT, Delhi and NPL have already used this facility for magneto-resistance and hall voltage measurement. At present measurement system is limited to 300K and at variable field 0- 6 Tesla but a variable temperature insert (VTI) is under development to cover the temperature range from 4.2 to 300 K.

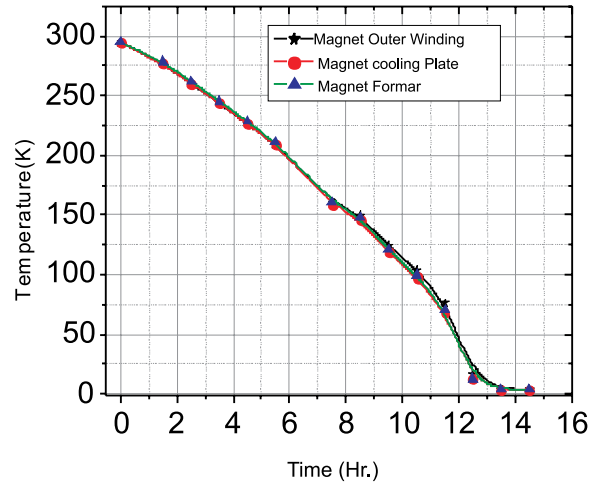


Fig. 9. Cool down profile of Magnet in CFMS

B. Superconducting Quadrupole Magnet Program for HYRA

A superconducting quadrupole doublet is planned in place of a room temperature doublet quadrupole magnet as a part of HYbrid Recoil Mass Analyzer (HYRA) to have better focusing power of the recoil nuclear fragments from nuclear collision experiment in the beam line. The doublet consists of eight superconducting coils. Twelve superconducting quadrupole coils have been wound using wet-winding technique. All the coils, before putting into the quadrupole cryostat, needs to be trained separately at LHe. So far, four coils have been trained in LHe in specially designed magnet vessel with vapor current leads integrated with existing STC.

The coils were charged upto 100A with maximum sweep rate 20A/min. After testing the remaining coils, all will be assembled in the magnet assembly consists of pole pieces and soft iron core. The cryostat components with reliquefaction system are already developed and procured.



Fig. 10. HYRA Quadrupole magnet coils

C. Collaborative work on Superconducting Fault Current Limiter

A project on development of single phase 3.3 kV and 1500 A by using High Temperature Superconducting Wire (HTSC) has been initiated by Central Power Research institute. Bangalore. IUAC, Delhi along with the other experts from IISc. Bangalore and IIT Kharagpur were invited by CPRI for a preliminary design evaluation meeting headed by Prof R Srinivasan. Official responsibilities for each institute are yet to be finalized and approved. A preliminary design calculation of length requirement and temperature rise (during fault) in adiabatic condition was completed with the available commercial wire from different manufacturers.

2.2.4 Home Made FPGA Based Instrumentation Development for LINAC Automation at IUAC

Among the various instrumentation developed for the LINAC automation, the first one is the development of a 16-channel digital linearizer unit for RF power read-backs and control which can display forward and reflected powers in a 40*4 display. In second development, 8 channel CAMAC programmable pulse generators (PPG) were designed, developed and used at the time of RF pulse conditioning of the SC resonators. A smart-encoder controllable single channel PPG was separately developed for manual pulse conditioning operations of Simple Test. A computer controlled drive probe controller was also developed to control the movement of 8 drive couplers of the resonator along with position sensor read back mechanisms for a few of them.

2.3 RF ELECTRONICS

A. Sarkar, S. Venkataramanan, B.K. Sahu, A. Pandey, & B.P. Ajith kumar

2.3.1 Status Report of the Multi-harmonic Buncher and associated jobs

The multi-harmonic buncher (MHB) was operated along with the low energy chopper (LEC) to provide 4 MHz pulsed beams to several LINAC users continuously for two months. Beams that were pulsed for the LINAC operation included ^{16}O , ^{18}O , ^{19}F and ^{30}Si . The FWHM of the beam bunch varied from 1 ns to 1.3 ns. The users were N. Badigar (Karnataka Univ), Savi Goyal (Delhi Univ.), I.Majumdar (TIFR), Varinderjit Singh (Punjab Univ.), Rohit Sandal (Punjab University), G. Mohanto (IUAC).

The system was also used to provide pulsed beams to several Pelletron users as well. The users were S. Nath (IUAC), Varinderjit Singh (Punjab Univ.), Rohit Sandal (Punjab University), Savi Goyal (Delhi Univ.). The beams that were pulsed included ^{16}O , ^{18}O , ^{19}F . The FWHM varied from 1 ns to 1.2 ns.

During the LINAC Run, some fluctuations in the beam bunch centroid was observed. A thorough test of the MHB electronics was done using beam simulation. The electronics was found to work satisfactorily. So the fluctuations were not from the electronics but from some other source. However, the problem was taken care of and the stability of the beam bunch centroid improved.

2.3.2 Software developments for LINAC control scheme

Improvement of the LINAC control scheme is undertaken for automation with minimum human intervention during beam acceleration. During beam acceleration and beam bunching/re-bunching, all the resonators have to be phase and amplitude locked with respect to the master clock. The fluctuation of resonant frequency due to mechanical vibrations, change of helium pressure etc. acts as the main disturbance to the stabilization process. This fluctuation occasionally is so large that the cavity goes out of lock thereby causing interruption in beam delivery. At this instant, RF power from the amplifier goes to maximum to stabilize the lock. The addition of python language interface has enabled us to write client programs for automatic monitoring and control of the phase lock condition. The program monitors the status of the phase lock condition as well as power from the RF amplifiers of all the cavities. Whenever the cavity goes out of lock and RF power from amplifier is high for more than a minute the phase and amplitude lock of the cavities are switched off to protect the rf drive cable. This software is used during the last LINAC run and found to be very useful for monitoring of amplitude and phase lock in automated manner.

2.4 BEAM TRANSPORT SYSTEM

A.Mandal, Rajesh Kumar, S.K.Suman, Mukesh Kumar and Sarvesh Kumar

Beam Transport System laboratory takes care of regular maintenance, design and development of Accelerator beam Transport System. This year the major thrust has been given for installation of facility and simulation of beam optics for HCI for various options. Different beam transport elements viz. quadrupole magnets, electrostatic quadrupoles, beam diagnostic elements etc are being developed for LEIBF and HCI. Power supplies for different magnets have been indigenously developed. Other than power supplies the group is actively involved in development of equipments for the others lab at IUAC. Details of development activities are summarised below.

2.4.1 New Low Energy Ion Beam Facility

The beam optics has been reported earlier. We have extended the ion optics calculations to see the focal position of multiple charge states for constant extraction

and accelerating potential for same current. A typical simulation for different charge state of Ar beam using code TRANSPORT is shown in the fig. 1a. The beam transmission was verified using multi-particle beam dynamics code TRACK and we have obtained 100% transmission in all the beam lines. The electrostatic quadrupoles are leak checked and tested for 10kV through high voltage connectors without any sparking. Analyzing cum switching magnet has been installed and aligned properly with respect to the beamlines. Magnetic steerers, scanners and electrostatic quadrupoles have also been installed in the beam lines for proper beam steering and focussing. All the beam line components have been installed as per layout design as shown in fig. 1b. The detail of installation is described elsewhere in this annual report.

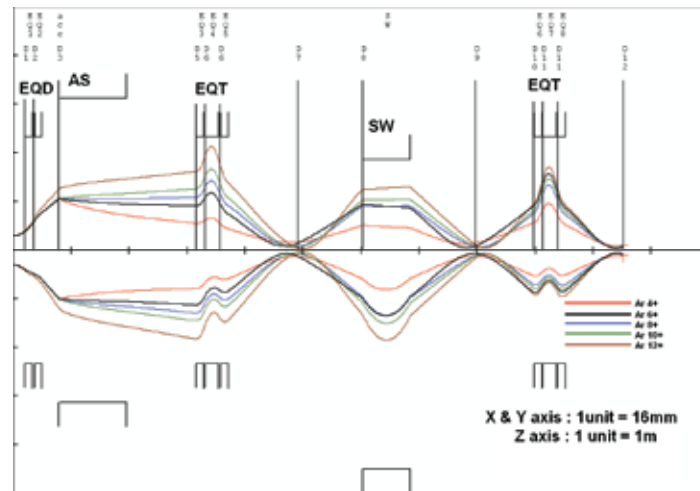


Fig. 1a. Beam optics of 90° line for multiple charge states of Ar using TRANSPORT

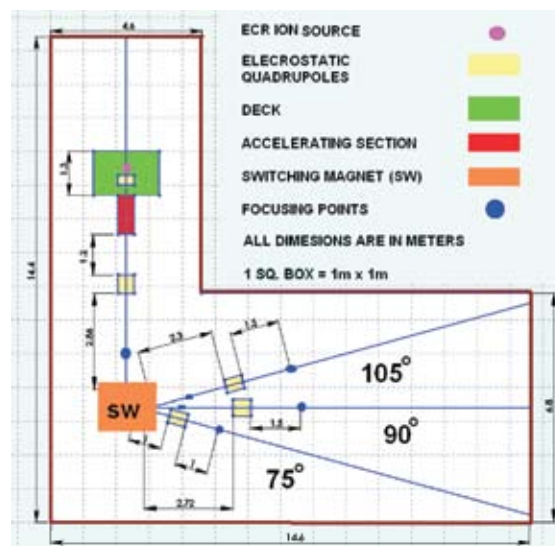


Fig. 1b. Layout of new LEIBF in Mat. Sc. Building (All dimensions are in mm)

2.4.2 Beam Optics of High Current Injector

The beam optics of high current injector is being divided into three different energy regime parts as follows with input parameters given in table-1.

- I. Low energy beam transport section (LEBT)
- II. Medium energy beam transport section, RFQ to DTL (MEBT)
- III. High energy beam transport section (HEBT)

Table 1 Ion optical parameters of different sections

Parameters	LEBT	MEBT	HEBT
Emittance (ϵ_x & ϵ_y) π mmrad, ϵ_z (π deg. keV)	100, 18	35, 300	12, 700
Mass to charge ratio (A/q)	6	6	6
Max. Magnetic rigidity (B ρ) Tm	0.09	0.36	1.15
Initial energy (E) keV/u	5	180	1800

I & II : Low and Medium energy beam transport section (LEBT and MEBT)

The beam optics of LEBT section has been reported earlier. This year it is checked along with RFQ by multiparticle beam dynamics code TRACK and observed 2% beam loss mainly inside RFQ as shown in fig. 2a. The ion optical parameters of all types of quadrupoles are given in table-2. The magnetic quadrupole doublet after the HTS-ECRIS has been fabricated and tested in the lab using Hall probe with appropriate current. Other four magnetic quadrupoles before the RFQ have been designed whose specifications with table-3.

Table 2. Parameters of Magnetic Quadrupoles

Parameters	After HTS-ECRIS (Doublet)	Before RFQ (Quartet)	RFQ to DTL (Singlets)
Effective length (mm)	78	156	106
Aperture Radius (mm)	39	39	26.5
Max. Field Gradient (T/m)	2.56	3.85	17

III : High energy beam transport section (HEBT)

The beam coming out of DTL is transported to supe buncher through HEBT section by following options in terms of different achromatic bend designs as per geometric layout.

Design-1 : 45-45, 90-90, 45-45

Design-2 : 45-45, 45-45, 45-45, 45-45

Design-3 : 45-45, 90, 45-45, 45-45

The transverse and longitudinal ion optics have been studied using GICOSY, TRANSPORT and TRACE 3D. The beam transmission in each design has been verified using code TRACK. The layout for design-1 has been reported earlier. The optical parameters of different elements of design-2 are given in table-4. All the magnetic field gradients of quadrupoles in this section are less than 10T/m. The layout of full HCI is shown in fig. 2b according to design-2 option of HEBT section.

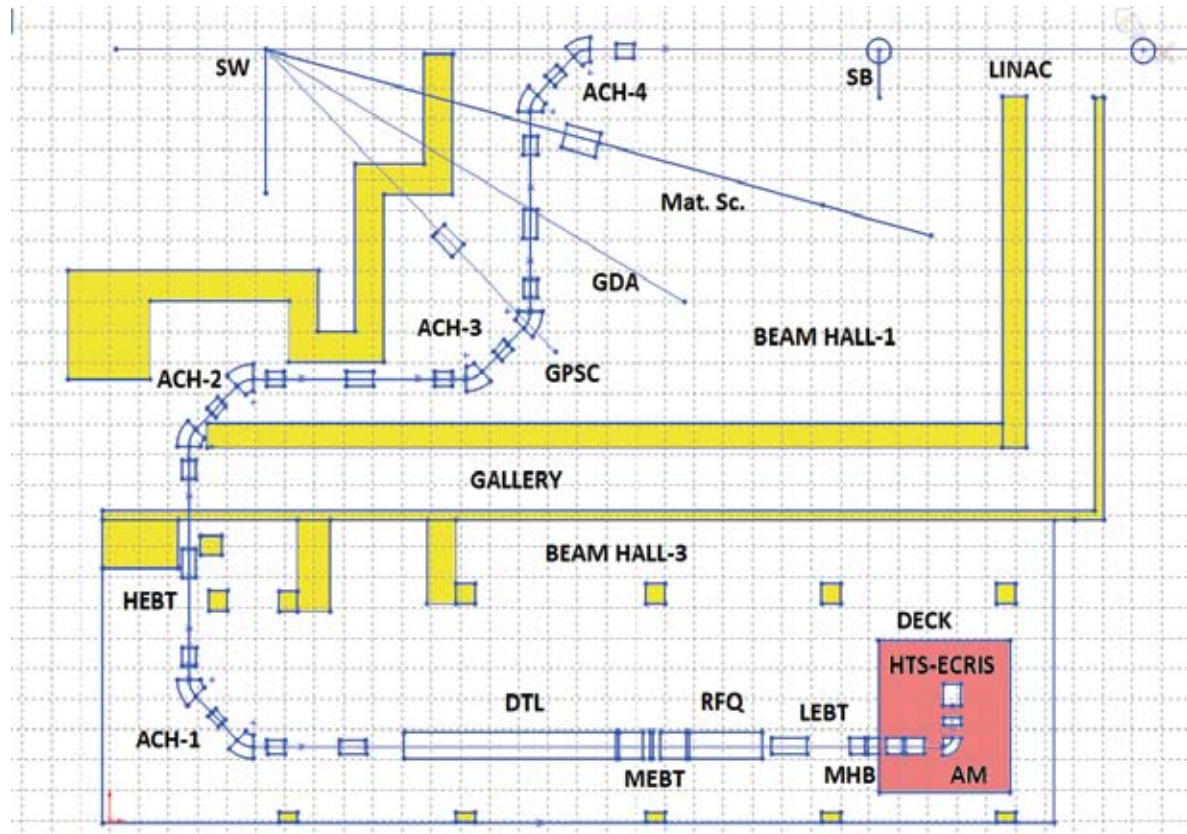


Fig. 2b. Layout of full HCI with design-2 of HEBT section (1 Sq. Box = 1m x 1m)

Table 4. Comparison of 45-45 deg. Achromatic bends in HEBT section

Parameters	Achromat-1	Achromat-2	Achromat-3	Achromat-4
No. of magnetic quadrupoles	10	6	6	6
No. of bending magnets	2	2	2	2
Shim angles of bending magnets (deg.)	15,15	33,33	26,26	26,26
Total length of achromats (mm)	6578	6528	7842	8113

2.4.3 High Voltage Power Supply for saddle field fast atom beam (FAB) source

DC High voltage power supply (3kV/200mA) for Saddle Field Fast Atom Beam Source has been designed and tested. It is currently operational with FAB source. The power supply is developed as part of the DST “Nano Mission” project at IUAC. Source power supplies must operate with frequent arcing, fast current demands or high slew rates. The switch mode technique is used for regulation, which is best suited to have fast slew rates. Because of high frequency operation it has relatively small output capacitance which results in small stored energy to the arc. The designed power supply is DC-DC converter operating at 50 kHz and has both constant-voltage and constant current regulation with automatic cross over. The power supply has an efficiency of 90%, output voltage ripple of 1% and fast dynamic response.

Special design features provided which are necessary for dynamic loads such as ion sources

- Voltage and current regulation with automatic crossover- for dynamic loads.
- High switching frequency to reduce stored energy- to have low power dissipation during arcing.
- Modular design - Any output voltage within 2kV to 40kV within 1kw power can be assembled using same PCBs & inductive components only by changing the multiplier board.

Operational Features

- Reversible output polarity.
- Remote programming and monitoring.
- Front panel control and metering.



Fig. 3. High Voltage Power Supply

Specifications

- Output voltage : 0- 3kV (adjustable by front panel 10-turn Pot. or external. 0-10V signal)
- Output Current : 0 - 200mA (adjustable by front panel 10-turn Pot. or external. 0-10V signal)
- Voltage regulation: For load transients from 10% to 100% typical deviation is 2% of output voltage with recovery to 0.1% in 1mS.
- Current regulation: 0.1% from short circuit to 3kV at any load current.
- Stability: 0.05% per 8 hours (current mode).

2.4.4 Three channel Linear high voltage ($\pm 2\text{kV}$) amplifier for Electrostatic steerer/scanner

Electrostatic ion beam steerers and scanners are planned in low energy ion beam facilities at IUAC to steer and scan the ion beam on the target. To accomplish the power supply requirement for both, a common unit has been specifically designed. It provides programmable high voltage bipolar DC output for steerers and high voltage bipolar triangular wave output for scanners. The unit is a standalone instrument consisting of three independent identical limited bandwidth high voltage ($\pm 2\text{kV}$) linear bipolar amplifiers, a controller module to generate local control signals and required HV bias supplies. The amplifiers output is linear from DC to 1kHz and can be programmed through entire range ($\pm 2\text{kV}$) using $\pm 5\text{V}$ input control signal. The amplifiers are optimized to drive capacitive loads.

Amplifier electrical specifications

- Number of channels: 3
- Input Impedance : $10\text{k}\Omega$
- Output voltage range: $\pm 2000\text{V}$
- Max. output current : 5mA
- I_o short circuit : 6.5mA
- Voltage Gain : 400 (fixed)
- Output noise : 6mV rms
- Full power band width : 1 KHz (resistive)



Fig. 4. Three channel Linear high voltage ($\pm 2\text{kV}$) amplifier

Operational Features

- Common unit for AC and DC applications.
- Single unit for X-axis, Y-axis and dog-leg plates.
- In-built programmable triangular-wave generator.
- Selectable remote and local control.
- Test-mode for calibration and troubleshooting.
- Scaled and buffered output voltage monitor.
- Modular assembly for easy maintenance.
- Floating output.
- Short-circuit protected output.

2.4.5 Thermoelectric Cooler (TEC) based rapid thermal cycler and Controller

A Thermoelectric Electric Cooler (TEC) based rapid thermal cycling system has been designed and developed. The system comprises of a controller and a sample holder whose temperatures can be rapidly and accurately controlled over a range of temperature from -25°C to $+100^{\circ}\text{C}$. This has been designed and developed to control the temperature of the crystals or samples during ion beam irradiation. The controller has two independent selectable operation modes, one to regulate temperature at any set point within the range and other to rapidly cycle the temperature between two set points. The heating and cooling capacity of the controller is 45Watts and 2 Watts for ΔT 10°C and 100°C respectively. Front panel setting provides independent control of heating and cooling ramp rate at max. $10^{\circ}\text{C}/\text{sec}$ and $3.5^{\circ}\text{C}/\text{sec}$ respectively, temperature limits for lower and upper temperature set points and monitoring all the temperatures.

Specifications & Features:

- Temperature Range from -25°C to $+100^{\circ}\text{C}$
- Double regulation loop (selectable)
- Auto-ramp control loop for rapid thermal cycling.
- PI control loop for temperature regulation at any set point within range.
- Independently settable heating (max. $10^{\circ}\text{C}/\text{sec}$) & cooling ramp rates (max. $3.5^{\circ}\text{C}/\text{sec}$).
- Independently settable temperature limits for Lower temperature set point and
- Upper temperature set point ($+50^{\circ}\text{C}$ to $+100^{\circ}\text{C}$)
- Lower temperature set point (-25°C to $+25^{\circ}\text{C}$)
- Front panel monitoring for TEC temperature, HS temperature, lower temperature set point, upper temperature set point, heating ramp rate, cooling ramp rate
- Remote monitoring: TEC temperature and Heat sink temperature ($100\text{mV}/^{\circ}\text{C}$).



Fig. 5. TEC based rapid thermal cycler

2.4.6 Steerer and Quadrupole magnet power supply development for upcoming HCI facility

In HCI facility large no of steerer and low power air cooled quadrupole magnets will be used. It has been decided to develop power supplies for these magnets in house. The requirement is as follows.

Types of magnets	Power supply rating	Quantity
Air-cooled quad magnets	10A, 10V (unipolar)	20
Steerer magnets	$\pm 5A, \pm 50 V$ (bipolar)	50

The circuit and mechanical design is in progress with the following design objectives:

- Regulation : Linear Series pass Transconductance Amplifiers
- Output-stage : Complimentary push-pull, class-A output stage, responds bi-directionally
- Crossover-distortion free output (transistors biased in class-AB).
- Control : Remote (CAMAC and Ethernet) and local front panel.
- Protections : Programmable over voltage and over current limits, over temp. magnet and PS.
- Cooling : Forced air cool.
- Size : 3U, 19" rack mount.

2.5 LOW ENERGY ION BEAM FACILITY

2.5.1 Electron Cyclotron Resonance Ion Source based Low energy Ion Beam Facility

U.K.Rao, Y.Mathur, P.Barua, A.Kothari, M. Archunan, Raj Kumar, P.Kumar, S.Kumar
C.P.Safvan, G.Rodrigues, A.Mandal & D.Kanjilal

I. Experiments performed using ECRIS based Low Energy Ion Beam Facility (LEIBF)

It has been working since 2000 and its performance has been satisfactory. In this year low energy ion beams of different charge states, in the range of a few KeV to a few MeV, were developed and delivered successfully for material science, atomic and molecular physics experiments. This energy range is most suitable for material engineering

and modifications. The production of highly charged positive ions is utilized to study atomic and molecular physics via ion-atom collision process. The list of experiments performed in the low energy ion beam facility is shown in the table 1 below.

TABLE 1. List of experiments performed

S.No	Details of Experiment	Affiliation
01	50 ,100 and 150 keV ion implantation on ZnO and Indium thin films at fluences 1.0×10^{17} and 1.0×10^{22} ions/cm ²	Subhashis Ghosh, JNU
02	Repairing of defects in MWCNT and SWCNT using 30 keV, N ⁺ and 80 keV, C ⁺ ions	Dilip Singh, IIT Guwahati
03	150 keV Ar ion irradiation on ZnO thin films , iron cobalt and teflon multi layers	Shantanu Ghosh , IIT Delhi
04	60 keV, argon ion irradiation on various types of GaAs surface for nanopatterning, highest fluence was 4×10^{18} ion/cm ²	T.Som , IOP Bhubhaneswar
05	60 keV Nitrogen ion implantation on NiTi, Ti6Al4V, 316 L and pure Ti for corrosion studied. Highest fluence was 1×10^{17} cm ²	M.R.Nair, Model college , Mumbai
05	100 keV N ⁺ , Ar ¹⁺ , Kr ¹⁺ ion irradiation on various polymers (PC , PET, PMMA , CR-39 , Kapton). Fluences 5×10^4 , 1.0×10^{14} , 5×10^{15} , 1.0×10^{16} , 2.0×10^{16} and 5×10^{16} .	Shyam Kumar , Kurukshetra University
06	250 keV, Argon ion irradiation at 60° on InP for ripple formation.	Indra Sulania IUAC
07	300 keV Argon implantation in Ag-silica nanocomposites prepared by ion exchange process	S.Mohapatra IPU , New Delhi
08	1 Mev, Kr ion irradiation on carbon stripper foils (floated on frame and TEM grid for structural change studies.	Sunil Ojha , IUAC
09	100 keV, H ⁺ ion implantation in GaN , SiGe and InGaAs at room temperature and liquid nitrogen. Fluence is 1.0 to 3.5×10^{17} ion/cm ² .	Rajendra Singh , IIT Delhi
10	50 keV , 100 keV Ar ¹⁺ ion irradiation on Si and GaAs for different fluences from 3×10^{17} to 5×10^{17} ions/cm ²	Tanuj Deswal , IUAC
11	50 keV, Ar ⁷⁺ , Ar ⁹⁺ beam utilized for atomic Physics to study time of flight for CH ₄ and CH ₃ OH	Jyoti , Delhi University
12	50 keV , Ar ¹⁺ ion irradiation on ZnS samples has carried out at different angles 10° , 30° and 40° from 1.1 o 4.5×10^{16} ions/cm ² .	Shiva Poojan Patel , Allaha- bad University
13	500 keV, Ar ³⁺ ion irradiation of Si nanorods	D. Kanjilal , IUAC
14	350 keV Ar ³⁺ ion irradiation on tungsten oxide samples to study surface modifications	BITS , Ranchi

S.No	Details of Experiment	Affiliation
15	70 keV , Ar ¹⁺ ion irradiation on Silicon bulk material has done study surface modifications	T. Som , IOP , Bhubaneswar
16	200 keV, Ar ²⁺ ion implantation on bi layer Silicone and cobalt	B.N.Dev , ICAS , Kolkata
17	450 keV , Ar ³⁺ ion irradiation on Ni – Mn – Sn samples at different fluence levels to study shift phase transformation temperature	Ritu Bishnoi, IIT Roorki
18	Measurement of neutron emission during 50 keV deuterium implantation in CaO-Pd-CaO multilayer samples	Nuclear Physics Division, BARC and IUAC, New Delhi

II. Maintenance Activities

This year we had major breakthrough in the maintenance front in repairing Traveling Wave Tube Amplifier (TWTA). The 250W 8GHz -18GHz, TWTA has gone bad two times in this year. Once it was the communication problem with the TWT interface board, which is happening after few hours of normal operation. It was due to noise in the low voltage power supply output (5V DC). After replacement of the module it has been working satisfactory.



(A) TWT Amplifier



(B) Traveling Wave Tube



(C) TWTA with modules open for tube replacement



(D) TWTA testing after tube replacement

Fig. 1. Traveling wave tube replacement in TWT amplifier

In the other major maintenance, the helix current of the Traveling Wave Tube (TWT) was found increasing and the TWTA was tripping due to tube arc fault. This was rectified by replacing its microwave Traveling Wave Tube and Remote Control Board. Since then it has been functioning well. The photographs of TWTA during microwave tube replacement are shown in figure.1

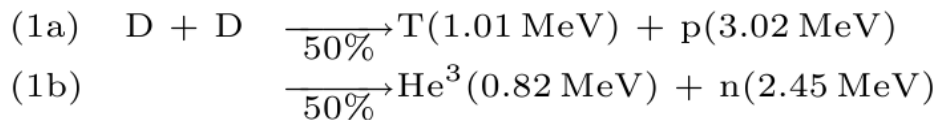
III. Details of few experiments

A). Measurement of neutron emission during 50 keV deuterium implantation in CaO-Pd-CaO multilayer samples

BARC, Mumbai - IUAC, Delhi collaboration

The objective of the experiment was to investigate neutron emission in d-d fusion during deuterium implantation in certain metal lattices like Palladium when the d/Pd ratio becomes close to 1.

In general d-d fusion follows the two paths:



While the Coulomb barrier for pure d-d fusion is ~ 200 keV, detectable reaction rate may occur even at much lower kinetic energies ~ 10 keV if there is enhancement of fusion due to the Coulomb screening in metal lattices. In this regard we irradiated a Pd metallic layer ($\sim 2000 \text{ \AA}$) sandwiched between two Ca-O layers of thickness ~ 7500 and ~ 7000 Angstroms respectively. The total number of Palladium atoms in the layer is $\sim 1.35 \times 10^{18}$. The average energy of the deuterium ions entering the Pd layer is ~ 15 keV with a range $\sim 920 \text{ \AA}$. Shown below (Fig.4) is a Monte Carlo simulation of the range distribution of Deuterium ions using the SRIM-2008 software. As can be seen, more than 90% of the implanted ions are in the Pd layer of thickness

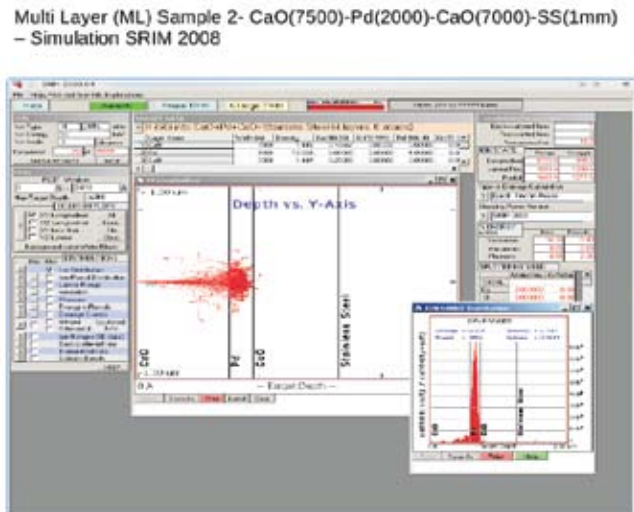


Fig. 2.

2000 A. At 10 micro ampere current for about 10 hours of irradiation one can achieve d/Pd ratio greater than 1.0.

Deuterium ions (produced by ECR source at the LEIBF facility of IUAC) were accelerated to the required energy (e.g. 50 keV) with an average current of about 10 micro ampere at the target. The beam profile was monitored using the Beam Profile Monitors (BPM) continuously and once on a scintillating medium. The experimental set-up consisted of four large area NE213 neutron detectors were placed around the scattering chamber at about 40 cm from the target. The energy threshold of ~ 0.5 MeV for neutrons was kept on all the four neutron detectors. A californium source spectrum is also taken to ensure proper n-gamma discrimination. A neutron gate was put using the software and the neutron rate was monitored on all the four detectors online.

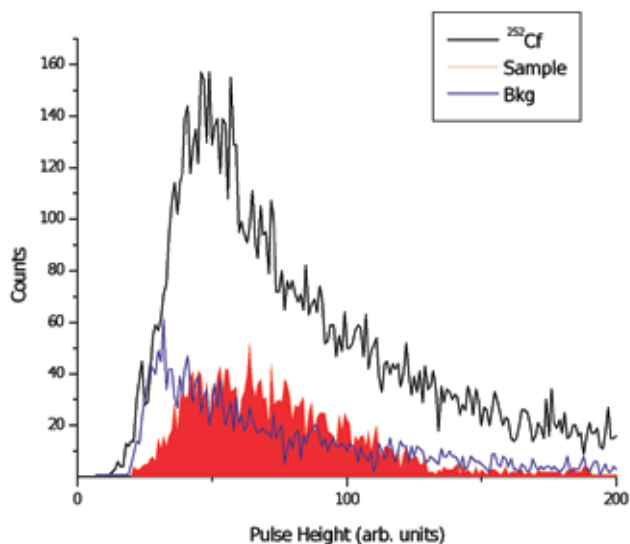


Fig. 3. Neutron gated pulse height spectrum

Fig. 3 shows the neutron gated pulse height spectrum for a given detector for three different counting situations, viz, the ^{252}Cf source, the background and during the time of implantation. As can be clearly seen, the shape of the spectrum during deuterium implantation is quite different from the background shape, and the ^{252}Cf spectrum. There are high energy neutrons produced during the irradiation corresponding to 2.45 MeV neutrons expected from d+d reaction. Detailed analysis is in progress.

IV. Facility upgradation

Some of the existing components have been shifted to the new LEIB building and most of the parts of the new facility have been completed. Preparation is going on in full swing for extraction and acceleration of the beam to the experimental beam lines. Few of the photographs especially of the ion source on the 400 kV high voltage platform and experimental beam lines are shown.



Fig. 4.



Fig. 5. Source on High Voltage Plat form



Fig.6. Experimental beam lines

2.5.2 High Temperature Superconducting ECRIS -PKDELIS and Low Energy Beam Transport (LEBT)

G.. Rodrigues, Y.Mathur, R.N.Dutt, R.Ahuja, U.K.Rao, D.Kanjilal & A.Roy

A. Source Operations



Fig. 1. (Left)A view of the 18 GHz HTS ECR-PKDELIS; (Middle) 18 GHz RF generator, HTS instrumentation electronics, cooling systems; (Right) post-analyser section

The operation of the source has not been very satisfactory this year due to cooling problems in the room coming mainly from the AC systems. The cooling requirements have been stringent on the cryo-cooler operations which should have an ambient temperature of 20 degrees. The reason is that the oil viscosity can change with temperature and can have a detrimental effect on the cooling capacity. Additionally, the injection cryo-cooler used to trip often and it was observed that the temperature setting was at 125 degree Fahrenheit. Comparing to the normal running cryo-cooler which had its temperature set at 160 degree Fahrenheit, the injection was reset to the same value of the extraction. The

18 GHz klystron needs proper inlet cooling, therefore, the cut-off temperature is set to 25 degrees for safe operation of the klystron. Various other sub-systems definitely require a low ambient temperature for smoother operations. It should be noted that the gas flow systems are very sensitive with temperature changes of a few degrees. We have observed the beam instabilities when the temperature rises above 3 or 4 degrees. In the near future, the gas flow control will be rectified to make sure that the gas flow is constant especially for the high charge state production.

Earlier we have observed that the DC break was getting burnt due to reflection of the rf power especially at rf powers of 1 kW. Most probably, a standing wave is generated at this position and causing the burn out. We have changed the position of the DC break slightly away from the rf window to avoid the standing wave. It was observed that this position was better with good stability. In the long term operation, the injection energy (from the source extraction) for the RFQ will be raised to 30 kV, therefore, it was important to go for a multi-step DC break for smoother operation. Due to the new design, water cooling is required to safely operate at 2 kW rf power with a maximum voltage of 40 kV (figure 2). The transmission co-efficient as a function of operational frequency is shown in figure 2.

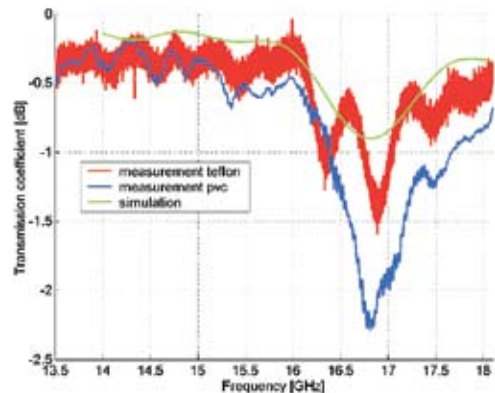
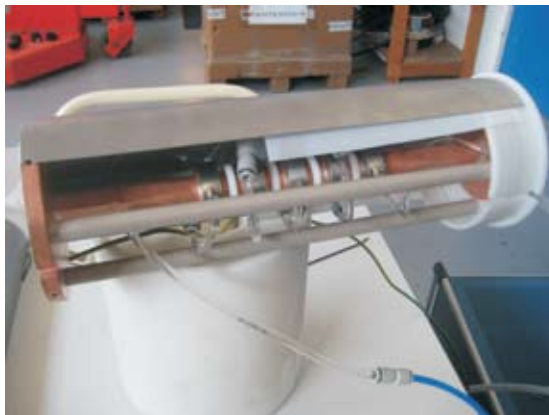


Fig. 2. (Left) View of the assembled multi-step DC break; (Right) transmission co-efficient as a function of operational frequency

B. Set-up for the measurement of the plasma potential of the PKDELIS ECR Ion Source

A major part of the development work was for developing a compact instrument for measuring the plasma potential of the ECR source. The plasma potential is an important measure of how the source is performing with respect to various tuning parameters of the source. The basic aim is to measure δV (the plasma potential) with respect to the source voltage while decelerating the beam through a retarding electric field. By varying δV over a range of values, the beam having the total energy of $q(V+\delta V)$ can be made to pass through the mesh at source voltage and be collected on a faraday cup. The power supply

should be able to compensate for the charging effects due to the beam impinging on the mesh. The compact system (figure 3) consists of a single collimator followed by a ring polarized to the source potential. The electric field uniformity is maintained between the collimator and the ring (covered with a mesh). It is shown in Figure 4 that if only the mesh is at source potential, the beam stops on the mesh. In the case when the beam is having a plasma potential of 10 V, the beam has just sufficient energy to go through the mesh and gets collected on the faraday cup. These plasma potential measurements will be important for defining the longitudinal beam optics of the HCI.



Fig. 3. View of the plasma potential measuring instrument

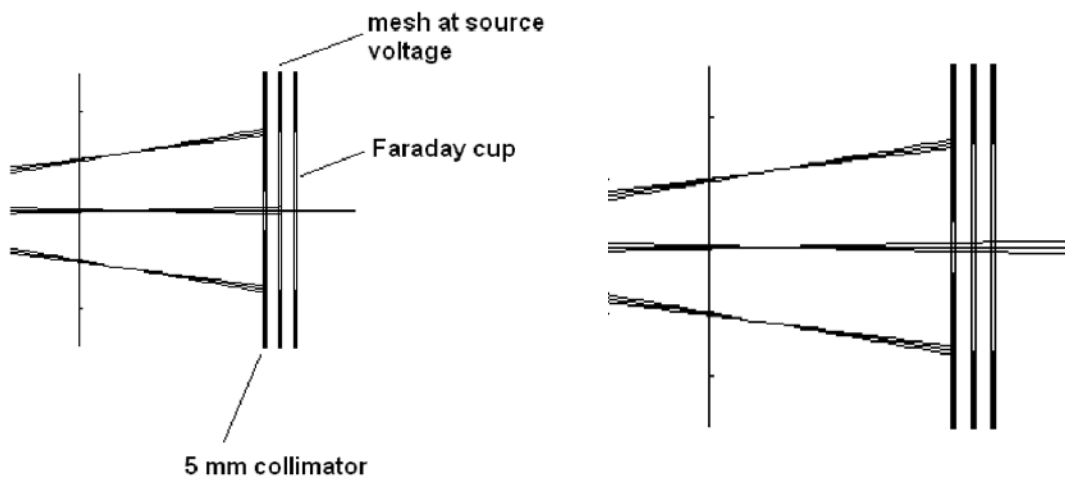


Fig. 4. (Left) Decelerating optics with plasma potential of 0 V; (Right) Decelerating optics with plasma potential of 10 V

C. Optics for the low energy beam transport (LEBT)

The optics from the source up to the post-analysed faraday cup has been looked into some detail and a comparison between the measurements and simulations show that the simulations predict quite well the observed transmissions. Extraction voltages around 15 kV to 20 kV have been found to be optimum for reasonable transmission and also for stable operation. However, higher extraction voltages beyond 20 kV causes over-focussing and the transmission through the system deteriorates. This was further verified during the emittance measurements. In Figure 6, the transmission is shown as a function of focus voltages at various extraction voltages.

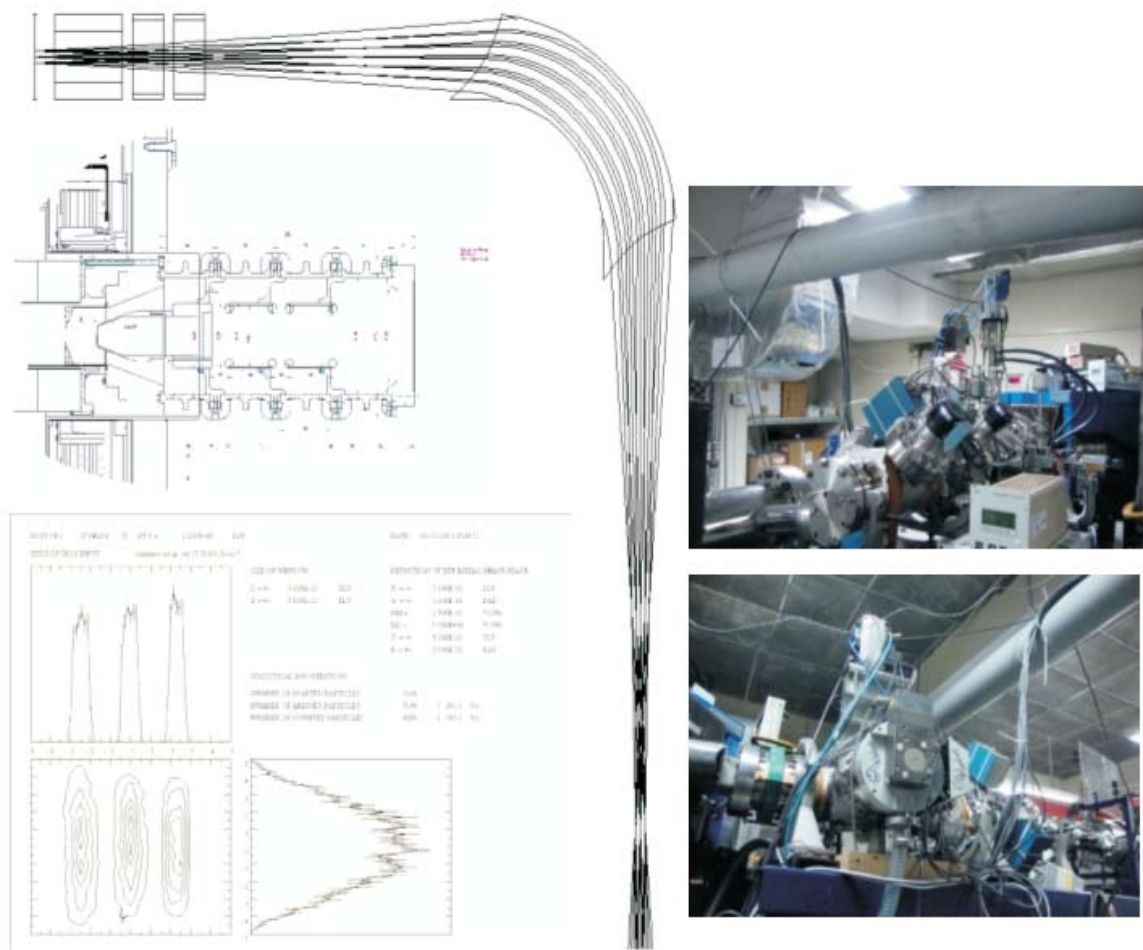


Fig. 5. Low energy ion optics through the LEBT

Note: (a) $d=37$ mm, except for the three cases @ 20 kV
 (b) puller and outer E. grounded
 (c) simulations for Ar $^{8+}$

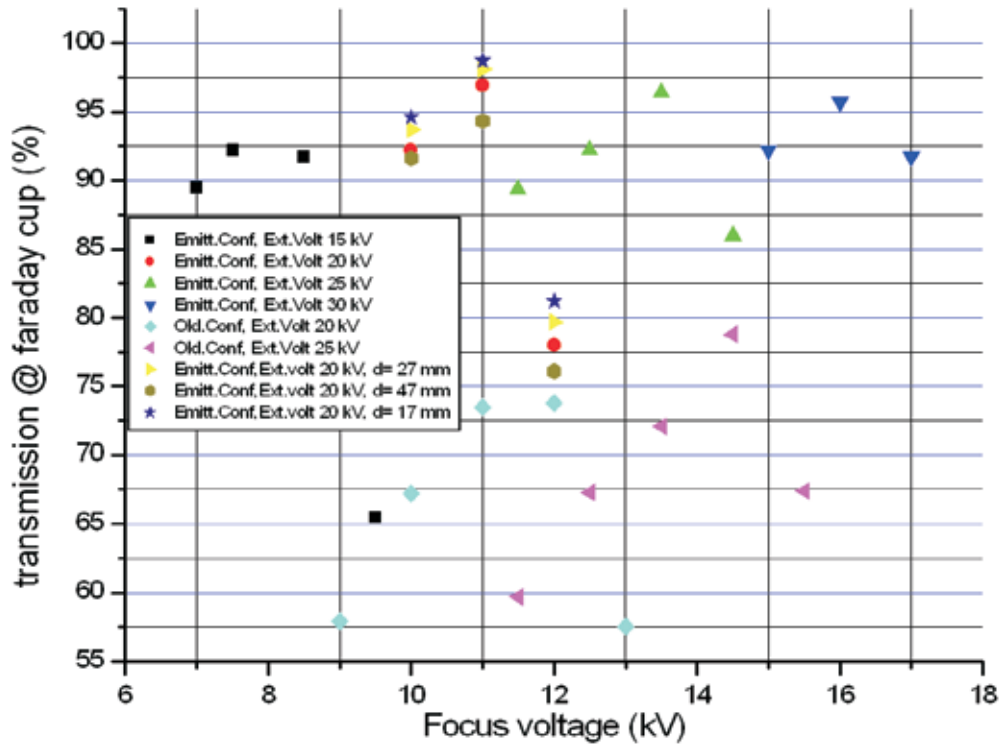


Fig. 6. Transmission as a function of focus voltage for various extraction voltages

D. Wireless Control and implementation for PCLI

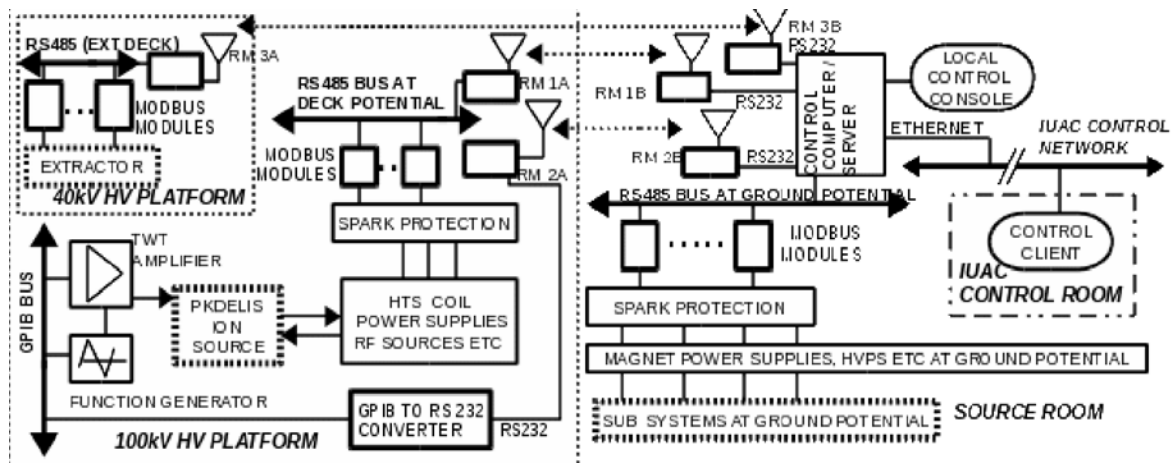


Fig. 7. Block diagram of the wireless based control system for the PKDELIS ECR ion source and LEPT

The source has been recently upgraded with an additional variable frequency functionality by incorporating a TWT amplifier and variable frequency function generator. The low energy beam transport section consists of the HTS PKDELIS ECR ion source, beam extraction system and a mass analyzer followed by a diagnostic system consisting of double slits, beam profile monitors and Faraday cups.

The centralized control system at IUAC is an ethernet TCP/IP based control scheme. A high level protocol on TCP/IP for data transfer / control is used in this system. The central control room houses the main control clients to be used by the operators. This client uses the TCP/IP protocol for communication with the server. The wireless control system for the HTS ECRIS- LEBT has been developed to provide both local operation and the ethernet TCP/IP based remote control. Distributed control topology has been adopted from the main control room. In the local control console of the source, functionality is enhanced by addition of graphs/charts and data logging functions. For interlocking, PLCs have been used. Automation work has been started. The control scheme of the PKDELIS HTS ECR ion source for the High Current Injector has been implemented using radio modems. The local and remote control features have been functional for more than three years.

E. Production of Intense Beams of Highly Charged Ions

3D simulation studies using RADIA code have been performed to optimise the magnetic holes in the high temperature superconducting electron cyclotron resonance (HTS-ECRIS) ion source for improving the extraction efficiency and beam intensities of highly charged ions. The magnetic field improvements using simple techniques like optimisation of iron regions was found to be economical . The extraction efficiency can be increased three-fold in the case of a hexapole magnet depending on the level of the uniformity of the fields in the high and low regions. This technique further minimises localized heating of the plasma chamber walls which can improve the vacuum conditions in an ECR ion source. The lifetime of synthetic high voltage insulators used between the plasma chamber and the cryostat can be increased further. For superconducting sources where the x-ray heat load poses severe problems during operation, such a reduction of heat load is of great significance. The typical triangular patterns of the plasma impact observed on the plasma electrode of HTS ECRIS at various tuning conditions are well reproduced by the simulations. After modification of the extraction system according to the simulations, preliminary experimental results had shown that the total beam current increased by a factor of 2 to 3. Beam stability aspects due to the larger currents extracted is being tried to improve further. In Figure 9, a ray tracing calculation is shown in 3D using SCALA without the effect of the axial magnetic field. The effect of the magnetic field is being

investigated and shape of the beam will determine its influence on the downstream focusing elements.

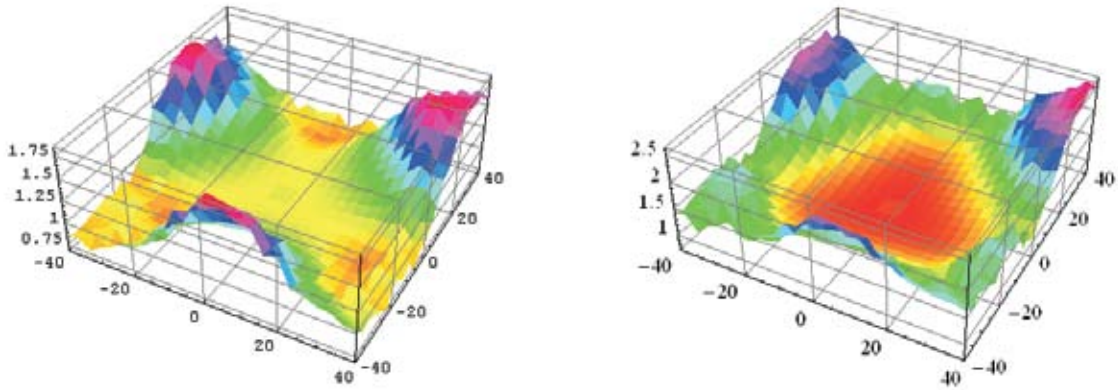


Fig. 8. (Left) Magnetic holes (Right) Optimised structure without magnetic holes

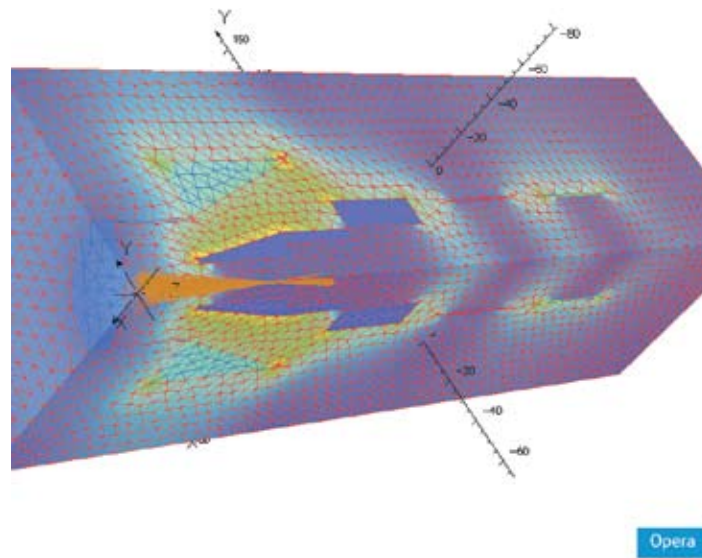


Fig. 9. SCALA calculation of the beam without the influence of the axial magnetic field

F. Finalization of positioning of sub-systems on the 100 kV High voltage platforms to prepare for injection into the RFQ and DTL accelerators

The various sub-systems that would be needed to operate the 18 GHz HTS ECR on a 100 kV high voltage platform have been finalized and positioned for smooth operation and at the same time to provide easy access during maintenance operations. The details of the 100 kV platform are shown in the following figure 10.

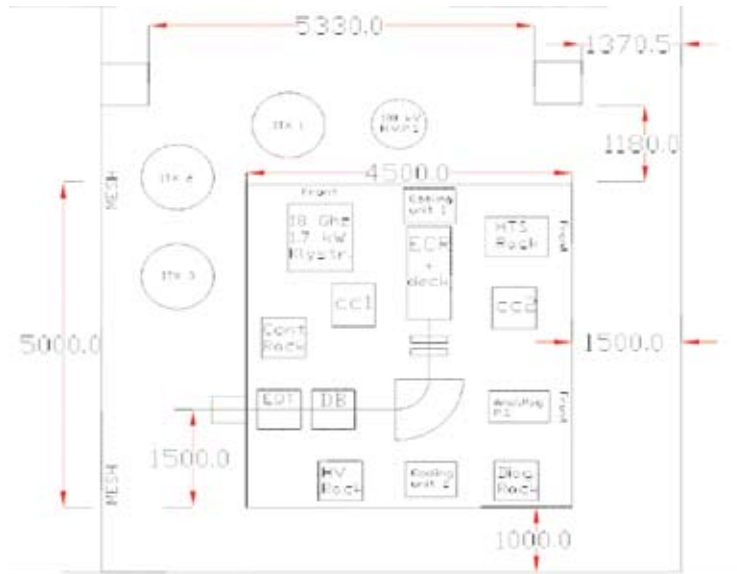


Fig. 10. Layout of the components related to the 18 GHz HTS ECR source on 100 kV high voltage platform

G. Development of 2.45 GHz ECR ion source

Due to demands for high intensities of singly charged ions for various kind of experiments in Materials Sciences and related applications, a low cost 2.45 GHz Electron Cyclotron Resonance (ECR) source has been designed which uses commercially available 800 W microwave ovens and permanent magnets. The total time related to the experiment for singly charged, ion implantation/irradiation on to the target sample can be reduced which is a major advantage. The major components of the ECR source are microwave system, plasma chamber and permanent magnets. Most of the components for this kind of source are being developed indigenously at IUAC.

The microwave system is sourced by a commercially available 800W magnetron. To reduce the cost of the ECR source we have used the magnetron of microwave ovens. A high power isolator or circulator will be used to protect the magnetron from load mismatch by directing the reflected power to the dummy load. Direction coupler will be used along with the RF power meters to monitor the forward and reflected power. The RF waveguide window will be used to provide vacuum isolation to the plasma chamber. DC break will be used for the high voltage isolation to the microwave source side from the plasma chamber. The schematic diagram of the 2.45 GHz ECR source system coupled to RF and beam extraction system is shown in figure 11. The designated waveguide for the operating frequency of 2.45GHz is WR340. Hence the microwave transmission line has been designed using WR340 waveguide sections. Figure 12 shows the photo of some of these indigenously developed components and the magnetron source. Various methods are being used for launching the RF power with efficient coupling in the chamber viz.

coaxial line, open ended waveguide, horn, slotted and helical antenna, ridged/ tapered waveguide to increase the plasma density. For example, the tapered waveguide or a ridged waveguide structure can be effectively used to increase the plasma density. Simulations using a 4 step ridged waveguide structure show improved electric fields in the plasma chamber as compared to normal waveguide structures for coupling the RF power to the plasma chamber is shown in figure 12. Figure 11 shows the operational modes where in the design case, $2a \sim d$. This source will produce intense beams of singly charged ions using a simple multi-electrode extraction system. It will cater the need of various materials science users for implantation experiments etc.

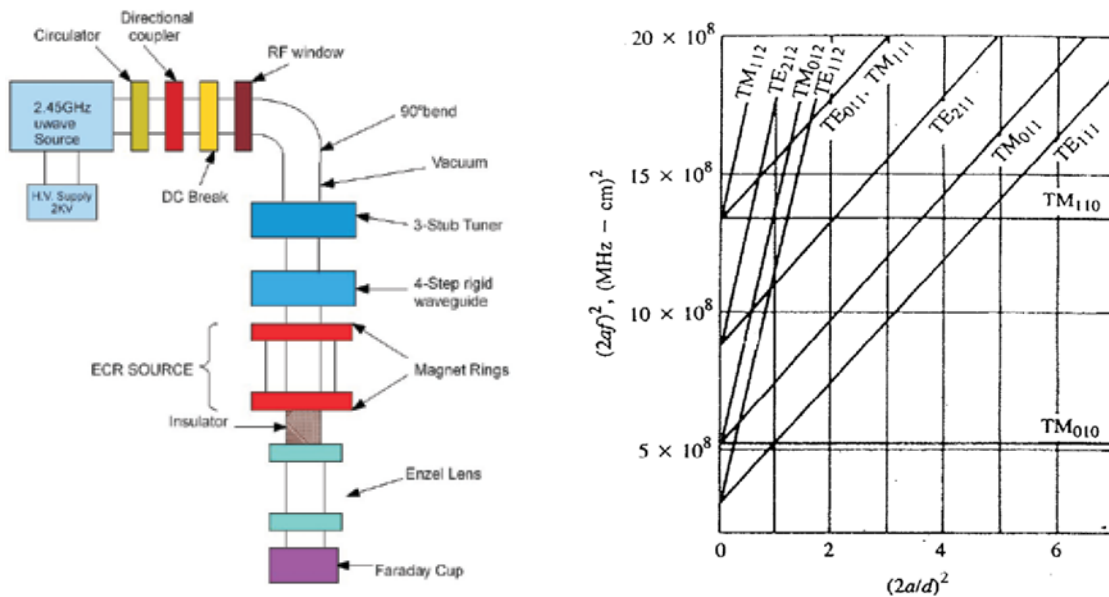


Fig. 11. (Left) Schematic Diagram of the 2.45 GHz ECR source with multi-electrode extraction system ; (Right) Resonant chart showing the operational modes



Fig. 12. 4 step quarter wave transformer coupled to the ECR cavity showing the TE_{111} mode; (Right) Magnetron and part of the assembled 2.45 GHz ECR source

REFERENCES

- [1] C. Bieth, S. Kantas , P. Sortais , D. Kanjilal , G. Rodrigues, S. Milward, S. Harrison , R. Mc Mahon, Nucl.Instrum.Meth., B 235 (2005) 498
- [2] D.Kanjilal, G.Rodrigues, P.Kumar, A.Mandal, A.Roy, C.Bieth, S.Kantas, P.Sortais, Review of Scientific Instruments,77,03A317 (2006)
- [3] A. Mandal,, G. Rodrigues, D. Kanjilal, Peter Brodt, Franz Bødker, Nuclear Instruments and Methods in Physics Research A 583 (2007) 219–227
- [4] R.Baskaran, T.S.Selvakumaran, G.Rodrigues, D.Kanjilal, A.Roy, Review of Scientific Instruments,79, 2008
- [5] A.Mandal, G.Rodrigues, D.Kanjilal, A.Roy, Physics Procedia 1 (2008)105, Proceedings of the Seventh International Conference on Charged Particle Optics
- [6] G.Rodrigues, P.S.Lakshmy, R.Baskaran, D.Kanjilal, A.Roy, Rev.Sci.Instrum. Vol 81,02A323 (2010)
- [7] G.Rodrigues, P.S.Lakshmy, Sarvesh Kumar, A.Mandal, D.Kanjilal, R.Baskaran, A.Roy, Rev.Sci. Instrum. Vol 81,02B713 (2010)
- [8] G.Rodrigues, P.S.Lakshmy, P.Kumar, A.Mandal, D.Kanjilal & A.Roy, Indian Journal of Cryogenics, Vol.34, No.1-4,2009, pg113
- [9] G.Rodrigues et al., 19th International Workshop on ECR Ion Sources, Grenoble, August 2010

2.6 STATUS OF DRIFT TUBE LINAC & RFQ ACCELERATOR

2.6.1 Fabrication, Modification and RF testing on Prototype Drift Tube LINAC at IUAC

B. P. Ajith kumar, J Sacharias, R. Mehta, R. V. Hariwal

Based on the electrical design, IUAC's first DTL tank is 84.5 cm in diameter and 38.7 cm in length with 11 gaps. All the solid modeling was done using SolidWorks and design was verified for structural and cooling using Ansys12.0. The strategy we adopted was to prototype all the DTL structures closest to the original design and to validate them by conducting various tests. Only after validating the required parameters successfully proceed for the actual manufacturing of the parts on expensive copper material. Table 1, gives details of all DTL resonators required.

Table 1: Specifications of Drift Tube LINAC

Tank #	Cells	Length (cm)	E Out (MeV/U)
1	11	38.5	0.32
2	13	73.4	0.55
3	13	94.4	0.85
4	11	86.5	1.15
5	11	99.2	1.46
6	9	81.6	1.80

PROTOTYPING

In order to have understanding of the manufacturing technology and skill we made the first prototype tank with stainless steel and welded explosively bonded Cu-SS material near the high current density areas of ridge base and end plates. Ridges and Stems were made of aluminum to do quick CNC machining of the parts in-house. During assembly and test we found that there were leaks in the bonding as well as on the aluminum casting of the Ridges. With this first prototype tank we carried out bead pull test and frequency measurements etc, whose results were satisfactory as reported earlier. We further modified the tank by avoiding bonded and cast materials, with modified ports as per our first DTL tank. In this prototype tank the end plates and ridges were made of low carbon steel to check the electroplating capability. Provision for additional cooling has been made by designing water sump near bottom side ridge base. The machined components were assembled in the second prototype tank, and again carried out low power RF tests.

A simple coaxial coupler was designed and installed in this tank. High power RF tests were done at 2.5 kW. Due to problem in RF amplifier we could not carry out rf test at higher power levels. All the results were satisfactory. By doing these exercises, one got expertise in assembly, frequency correction by machining and cooling solutions. Presently this tank is ready to go for electroplating and after that we plan to do the high power test using couplers and tuners.

MANUFACTURING OF FIRST DTL TANK

Fabrication of the first DTL resonator is presently underway at vendors site in Canada. The tank is made out of forged cylinder of low carbon steel with wall thickness of 3.8 cm. End plates are made of solid copper having 3.0 cm thickness. The tank was tested for vacuum and found a deflection of 0.4mm during the evacuation. Tank was copper plated as per the RF requirements. Ridge base was machined after electroplating to get a flat and parallel surface. Meanwhile we fabricated copper ridges and stems for this tank at IUAC. Machining allowance of 1.5mm is provided on the stems for alignment. The assembly and power



Fig. 1. DTL Tank # 1

testing of the tank will be done after testing all the elements in the test tank. Figure 1 shows the tank during machining and before copper plating at vendors site.

FABRICATION EXPERIENCE

Machining : It was decided that all the internal parts shall be made in at IUAC using in house CAM and CNC facilities of workshop. This made prototyping and modification faster and efficient. Special attempt was made for cooling of the tanks as well as the end plates. Stiffeners are provided to minimize the deflection. We have fabricated both cylindrical and flat type ridge bases. Tanks were also fabricated to mount the ridges with cylindrical and flat surfaces. Cylindrical base ridge has advantage that we can avoid machining of tank ridge base after copper plating.

Assembly : For assembly we used assembly fixtures as well as portable arm type CMM. The stems are bolted with ridges at their final locations and we achieved alignment accuracy better than ± 50 microns. O-ring seals were made to seal the water channels. Fully assembled resonator was then vacuum leak tested at leak rate 10^{-9} mbar-l/sec. Bal seals are provided on the tank to end plate joints for the better RF conductivity.

Beam dynamics for the DTL has been optimized for the desired energy range. Electromagnetic design of the IH structure has been done and verified by making measurements on a full scale prototype fabricated. The frequency and voltage distribution results are in agreement with the calculations.

2.6.2 High Power RF Tests On The Modulated Prototype RFQ Accelerator

C.P. Safvan, Sugam Kumar, R. Ahuja, A. Kothari, R.V. Hariwal, D. Kanjilal

A prototype of four-rod RFQ with operating frequency of 48.5MHz is designed and constructed as an accelerator section of High Current Injector (HCI) system to accelerate ions with A/q of 6 from 8keV/A to 180keV/A. The ion beams produced by the ECR (PKDELIS) source will be injected into the RFQ and be further accelerated to just above 2MeV/A by a drift tube LINAC (DTL) working at room temperatures, velocity matched beam with $\beta = 0.08$ will be injected into superconducting LINAC, which will further accelerate the ions to 5MeV/A. An initial modulated 1.17m section of the RFQ is designed and constructed to determine the specifications for final RFQ accelerator which will be 2.5m in length.

The length of the electrodes in the prototype is 1.17 meters with bore radius of 4 mm. The whole electrode assembly is inserted in RFQ cavity of internal dimensions 1194 x 500 x 355 mm. The material of electrodes and electrodes supporting posts is all copper

while base plate and chamber is of stainless steel. Assembly of vanes has been achieved within an accuracy of 100 microns. The chamber can hold a typical vacuum level of 1×10^{-7} torr. To improve the quality factor the inner surface of the chamber as well as the base plate is copper plated with a plating thickness of 70 microns.

The low power RF test has been done to measure the following RF parameters which are essential to check the performance of the cavity. The perturbed resonance frequency (f), quality factor (Q) and unperturbed resonance frequency (f_0) are measured with a network analyser, while capacitive variation method is used to determine the shunt impedance (R_{sh}) of the cavity. The electric field distribution along the length of the cavity and the quadrupole symmetry is checked by Bead Pull method. We used a fully automated bead puller system. Self-exciting loop is used to minimise the possible long-term temperature drift while measuring the frequency shift. Results indicate that the distribution of the electric field is symmetrical within the beam radius and tend to asymmetrical in region greater than the beam radius.

The RF test has been done on modulated vanes with and without copper plating of the chamber walls and base plate. The RF result stainless steel chamber and copper plated chamber is summarized separately in table 1 and table 2 respectively. Comparison result indicates that the copper plating has improved the quality factor from 2355 to 3112. This brings down the power required to generate 70kV inter-electrode voltage from 43kW/m to design value of 30kW/m

Table 1. The RF characteristics of modulated 4-rod RFQ with stainless steel chamber

RF parameters	Designed Value	Simulated	Experimental
f_0	48.5 MHz	-	53.02
Q	-	4000	2355
R_{sh}/Q	-	-	23.65
R_{sh}		80k-ohm	55.7k-ohm
P_{in}	-	30kW/m	43kW/m

Table 2. The RF characteristics of modulated 4-rod RFQ with copper plated chamber

RF parameters	Designed Value	Simulated	Experimental
f_0	48.5 MHz	-	53.02
Q	-	4000	3112
R_{sh}/Q	-	-	26.37
R_{sh}		80k-ohm	82.08k-ohm
P_{in}	-	30kW/m	29.85kW/m

The high power RF tests are to check the resonant frequency and temperature stability of the four-rod RFQ. To maintain the temperature stability of the cavity during high power run, independent cooling water channels are allocated for the RFQ electrodes and posts. A 35kW commercial RF amplifier of operating frequency 48.5MHz with ± 1 MHz bandwidth has been used. Before feeding power into the cavity the RF amplifier was tested with dummy load up to 10kW. An air cooled RF power coupler is designed to feed power in the cavity. Coupler is made of 500mm long copper tube whose inner and outer diameter is 4 and 6mm respectively. To minimise the reflected power, coupling coefficient is optimised at 0.84.

Base pressure of 1.6×10^{-7} Torr was maintained before feeding RF power. We encountered vacuum fluctuation due to degassing in the cavity in the beginning of the power feeding, which was cured when degassing stopped. After this the vacuum pressure was below 1.2×10^{-6} Torr at any RF power level. We fed 20kW in the cavity in small steps. The resonant frequency was found to decrease with increasing RF power. To minimise the power reflected from the coupler we continuously tuned the operating frequency of the RF Amplifier. The temperature of the cooling water rises marginally.

Presently we are working on the designing of the RF power coupler before the beam test. Tuner and its electronics yet have to be designed.